IASLC

Check for updates

Genomic and Transcriptomic Characterization of Relapsed SCLC Through Rapid Research Autopsy

Hui-Zi Chen, MD, PhD,[a,b] Russell Bonneville, BS,[c,d] Anoosha Paruchuri, PhD,[c]
Julie W. Reeser, PhD,[c] Michele R. Wing, PhD,[c] Eric Samorodnitsky, PhD,[c]
Melanie A. Krook, PhD,[c] Amy M. Smith, BS,[c] Thuy Dao, BS,[c] Jharna Miya, MS,[c]
Walter Wang, BS,[e] Lianbo Yu, PhD,[f] Aharon G. Freud, MD, PhD,[g]
Patricia Allenby, MD,[h] Sharon Cole, MD,[i] Gregory Otterson, MD,[c,j]
Peter Shields, MD,[c,j] David P. Carbone, MD, PhD,[c,j]
Sameek Roychowdhury, MD, PhD[c,k,*]

[a]Division of Hematology and Oncology, Department of Medicine, Medical College of Wisconsin, Milwaukee, Wisconsin
[b]Genomic Sciences and Precision Medicine Center and Cancer Center, Medical College of Wisconsin, Milwaukee, Wisconsin
[c]Division of Medical Oncology, Department of Internal Medicine, Comprehensive Cancer Center, The Ohio State University, Columbus, Ohio
[d]Biomedical Sciences Graduate Program, The Ohio State University, Columbus, Ohio
[e]Medical Scientist Training Program, The Ohio State University, Columbus, Ohio
[f]Department of Biomedical Informatics, The Ohio State University, Columbus, Ohio
[g]Division of Hematopathology, Department of Pathology, The Ohio State University, Columbus, Ohio
[h]Division of Autopsy Services, Department of Pathology, The Ohio State University, Columbus, Ohio
[i]Orion Cancer Care, Inc., Blanchard Valley Health System, Findlay, Ohio
[j]James Thoracic Center, Comprehensive Cancer Center, The Ohio State University, Columbus, Ohio
[k]The James Cancer Hospital, The Ohio State University, Columbus, Ohio

ABSTRACT

Introduction: Relapsed SCLC is characterized by therapeutic resistance and high mortality rate. Despite decades of research, mechanisms responsible for therapeutic resistance have remained elusive owing to limited tissues available for molecular studies. Thus, an unmet need remains for molecular characterization of relapsed SCLC to facilitate development of effective therapies.

Methods: We performed whole-exome and transcriptome sequencing of metastatic tumor samples procured from research autopsies of five patients with relapsed SCLC. We implemented bioinformatics tools to infer subclonal phylogeny and identify recurrent genomic alterations. We implemented immune cell signature and single-sample gene set enrichment analyses on tumor and normal transcriptome data from autopsy and additional primary and relapsed SCLC data sets. Furthermore, we evaluated T cell-inflamed gene expression profiles in neuroendocrine (*ASCL1, NEUROD1*) and non-neuroendocrine (*YAP1, POU2F3*) SCLC subtypes.

Results: Exome sequencing revealed clonal heterogeneity (intertumor and intratumor) arising from branched evolution and identified resistance-associated truncal and subclonal alterations in relapsed SCLC. Transcriptome analyses further revealed a noninflamed phenotype in neuroendocrine SCLC subtypes (*ASCL1*, *NEUROD1*) associated with decreased expression of genes involved in adaptive antitumor immunity whereas non-neuroendocrine subtypes (*YAP1*, *POU2F3*) revealed a more inflamed phenotype.

Conclusions: Our results reveal substantial tumor heterogeneity and complex clonal evolution in relapsed SCLC. Furthermore, we report that neuroendocrine SCLC subtypes are immunologically cold, thus explaining decreased responsiveness to immune checkpoint blockade. These results suggest that the mechanisms of innate and acquired therapeutic resistances are subtype-specific in SCLC and highlight the need for continued investigation to bolster therapy selection and development for this cancer.

Introduction

SCLC is a lethal neuroendocrine malignancy accounting for 13% to 15% of new lung cancer cases annually worldwide.[1,2] Most patients with SCLC present with initially chemotherapy-sensitive disease, but almost all will experience progression or relapse leading to death. In 2019, combination chemotherapy and immunotherapy was approved by the Food and Drug Administration as first-line treatment for metastatic SCLC,[3,4] with modest 2-month improvement in survival compared with chemotherapy alone. For decades, topotecan was the only Food and Drug Administration–approved second-line chemotherapy with objective response rate of 10% to 20%,[5] until lurbinectedin was granted accelerated approval in 2020 on the basis of a phase 2 trial revealing 35% objective response rate.[6] Despite these recent approvals, there is an urgent need to develop more effective therapies for advanced SCLC.

Key studies in the past decade have profiled the mutational landscape of primary SCLC, driven by *TP53* and *RB1* inactivation.[7–9] Furthermore, distinct SCLC subgroups have been identified on the basis of the expression of key transcription factors including ASCL1 and NEUROD1.[10,11] How each SCLC subtype confers different clinical phenotypes and differential response to anticancer therapies is under active investigation,[12] with the goal of delivering precision therapy to patients with SCLC by matching each SCLC subtype to specific treatments.

Molecular characterization of relapsed SCLC has been hampered by tissue scarcity owing to rapid clinical deterioration of patients with relapse. Therefore, unlike for primary SCLC, less is known on the genomic and transcriptomic landscapes of relapsed SCLC and mechanisms that mediate therapeutic resistance, although recent nonautopsy studies on relapsed SCLC have begun to address this knowledge gap. For example, Gardner et al.[13] used patient-derived xenografts of paired chemosensitive and chemoresistant SCLC tumors to elegantly reveal that acquired chemoresistance occurred through epigenetic silencing of a DNA damage repair factor, *SLFN11*. Wagner et al.[14] performed genomic profiling on a cohort of patients with relapsed SCLC and identified recurrent Wnt pathway alterations as a mechanism of acquired chemoresistance. Weiss et al.[15] performed genome-wide exome and RNA sequencing (RNA-seq) on 12 patients with SCLC who relapsed after platinum-based chemotherapy. Aside from driver mutations in *RB1* and *TP53*, the authors identified few recurrent targetable genomic alterations in this cohort of patients. Finally, an important study by Stewart et al.[16] performed single-cell sequencing of circulating tumor cells and circulating tumor cell-derived xenografts from patients with platinum-sensitive and refractory SCLC and revealed an association between increased intratumoral heterogeneity and chemoresistance. The latter study is one of the first nonautopsy studies to directly evaluate intratumor heterogeneity in advanced SCLC. Overall, however, further study of relapsed SCLC is needed to identify additional targetable mechanisms underlying therapeutic resistance, including resistance to immunotherapy, which is now approved for frontline treatment in the metastatic setting.

The use of tumor specimens from rapid research autopsy has accelerated the study of tumor heterogeneity and acquired resistance in advanced cancer.[17] To our knowledge, this is the first study to perform whole-exome and transcriptome profiling of advanced SCLC through research autopsy. From exome sequencing, we inferred intertumor and intratumor clonal heterogeneity arising from branched evolution and transcriptome analyses supported the subtype-specific suppression of adaptive antitumor immunity in primary and advanced SCLC. Our results provide new insights into the subclonal architecture of advanced SCLC and identify new potentially targetable pathways involved in antitumor immune responses.

Materials and Methods
Rapid Research Autopsy

Informed consents were obtained from five patients with advanced SCLC to participate in an institutional

review board–approved clinical study for tumor profiling by next-generation sequencing and body donation (NCT02090530).[17,18] Deceased patients were transported to The Ohio State University Regional Autopsy Center, where research autopsy for tumor procurement was performed no more than 16 hours after the passing of the patients. Computed tomography imaging when available was used to guide procurement from organs with cancer. After autopsy completion, the deceased were transported to a designated funeral home within 24 hours.

Tumor DNA/RNA-Seq

Samples with tumor cell content greater than 60% and without substantial necrosis were selected for next-generation sequencing analyses. Genomic DNA and total RNA were extracted using Qiagen kits per manufacturer's protocol. Libraries were prepared after established protocols (TruSeq Stranded Total RNA with RiboZero Gold, Illumina),[18,19] enriched with the xGEN Exome Research Panel version 1.0 (IDT) and sequenced on an Illumina HiSeq 4000.

Circulating Tumor Sequencing

Circulating tumor DNA (ctDNA) sequencing was isolated using QIAamp Circulating Nucleic Acid Kit (Qiagen) per manufacturer's protocol. An input of 300 ng was used to generate libraries for paired-end sequencing on a NextSeq instrument achieving median coverage of approximately $\times 500$.[20]

Somatic Mutation and Copy Number Variant Calling, Clonal Inference, and Mutational Signatures

These bioinformatics analyses were performed as previously described.[18] Briefly, sequencing reads were aligned to human genome build 19 (hg19) using Burrows-Wheeler Aligner (bwa),[21] deduplication with Picard (https://github.com/broadinstitute/picard), and base quality score recombination and realignment around insertion and deletion (indels) with GATK.[22] Variants were called with VarScan2[23] and allele-specific copy number variations (CNVs) with FALCON.[24] Clonal inference was performed using Canopy,[25] and mutational signatures were inferred with deconstructSigs.[26] Bradley-Terry modeling was used to estimate relative ordering of mutations in the phylogeny branches of autopsy patients with SCLC as previously described.[18]

Significantly Mutated Gene Analysis

Significantly mutated gene (SMG) analysis was identified using MuSiC version 2.0,[27] with default settings.

Variants from all tumor samples were merged per patient by taking the highest variant allele fraction. The p value and false discovery rate (FDR) estimates are on the basis of three tests including Fisher's combined p value test, convolution test, and likelihood ratio test methods. For a specific gene, if FDR for at least two of these tests is less than or equal to maximum FDR, then it was called as a SMG. For all five SCLC research autopsy patients, the maximum FDR cutoff was set to 0.05.

Driver Mutation Prediction

CHASM was used to identify statistically likely driver mutations.[28] Missense variants were merged per patient and deduplicated before input to CHASM.

Transcriptome Analysis

RNA-seq reads were aligned to hg19 using HISAT2,[29] and fragments per kilobase per million reads and transcript reads per million (TPM) were calculated with StringTie[30] as described in the Supplementary Methods.

Single-Sample Gene Set Enrichment and Immune Signatures

Single-sample gene set enrichment (ssGSEA) version 2.0 was implemented with default settings in R.[31] Gene sets assayed were obtained from PanCancer Immuno-Oncology 360 and Tumor Signaling 360 from Nano-String. Immune signatures (ImSigs) were run using TPM values with default settings to identify enrichment of 10 ImSig.[32] Linear mixed-effects models and t statistics were used to model ssGSEA and ImSig scores by allowing correlation among multiple samples within each patient. Tukey's method was used for adjusting p values of multiple comparisons of enrichment scores from ssGSEA using NanoString gene sets and scores from ImSig.

External SCLC RNA-Seq Data Sets

RNA-seq data of primary and relapsed SCLC and normal lung tissue were obtained from four previous publications.[8,14,15,33] Of these four data sets, one had paired primary SCLC and normal lung samples,[8] whereas the rest contained either exclusively tumor[14,15] or normal samples.[33] Non-SCLC RNA-seq data were downloaded from the The Cancer Genome Atlas data portal (https://portal.gdc.cancer.gov/). We randomly chose a subset of 60 and 49 tumor-normal paired samples of lung adenocarcinoma and squamous cell carcinoma, respectively, for ssGSEA and ImSig analyses.

Molecular Subtyping of SCLC Samples

SCLC subtype classification was performed after a previously published method.[34] Briefly, the samples were classified on the basis of defining thresholds

($\log_2$[fragments per kilobase per million $+$ 1]) for transcription factors *YAP1* (2.5) and *POU2F3* (2.5). Samples were classified as ASCL1 or NEUROD1 subtype on the basis of relative expression of these genes, with minimum required difference of 1. The above-mentioned method was unable to classify all samples included in this study; therefore, remaining samples were assigned to SCLC subtypes on the basis of the gene (*ASCL1*, *NEUROD1*, *YAP1*, or *POU2F3*) with highest expression (TPM) value. When expression difference was less than twofold between *ASCL1* and *NEUROD1*, samples were classified as dual-positive ASCL1/NEUROD1. *ARG2* expression between subtypes was compared using two-tailed unpaired *t* tests.

T Cell-Inflamed Gene Expression Profile Scores and Heatmaps

TPM values for genes in the housekeeping (n = 11) and predictor (n = 18) sets were converted into count-equivalent values, and gene expression profile (GEP) scores were computed as previously described[35] and as detailed in the Supplementary Methods. Heatmaps of log-transformed TPM values of the 18 genes in the T cell-inflamed GEP were generated using Qlucore Omics Explorer (Qlucore AB) version 3.6.

Results

Demographic and clinical information of the five patients with SCLC who underwent research autopsy is presented in Table 1. All had metastatic SCLC at diagnosis and received multiple lines of treatments, including first-line cisplatin or carboplatin and etoposide as autopsies were performed before the approval of atezolizumab and durvalumab. All patients responded to first-line chemotherapy but relapsed within 1 to 5 months of completing the last treatment cycle. Three patients received immunotherapy subsequently but were nonresponders. The time from diagnosis to death ranged from 12 to 25 months. Numerous metastatic tumors from four to five different organs were procured through autopsy of each patient. A total of 60 metastatic tumor samples were selected for whole-exome sequencing (WES) and 30 tumor samples for RNA-seq (Supplementary Data 1). Pretreatment samples were included for WES and RNA-seq when available. Matched normal lung tissue was available for RNA-seq from two autopsy patients (Supplementary Data 1).

Genomic Alterations in Relapsed SCLC

WES revealed high tumor mutational burden (TMB) in our SCLC tumor samples, ranging from 5.7 to 29.8

Table 1. Demographics and Clinical Histories of Relapsed Small Cell Lung Cancer (SCLC) Patients Who Underwent Research Autopsy

	SCLC 1	SCLC 2	SCLC 3	SCLC 4	SCLC 5
Gender	Female	Female	Male	Male	Female
Age	59	54	75	62	64
Ethnicity	Caucasian	Caucasian	Caucasian	Caucasian	Caucasian
Smoking (pack years)	60	20	60	45	47
Stage at diagnosis	Extensive	Extensive	Extensive	Extensive	Extensive
Radiation	PCI[a] and palliative	PCI	PCI	Palliative	PCI
1st line therapy	Cisplatin & etoposide x6	Carboplatin & etoposide x4	Cisplatin & etoposide x6	Carboplatin & etoposide x4	Carboplatin & etoposide x4
Best response to platinum	PR[b]	Mild/mixed response	PR	PR	PR
Subsequent therapies received	Topotecan	Irinotecan Rova-T[c] Paclitaxel	Irinotecan Nivolumab	Immunotherapy[d] Irinotecan	Immunotherapy[d] Irinotecan Rova-T[c] Paclitaxel Gemcitabine
Time from diagnosis to death	23 months	12 months	25 months	12 months	22 months
# Metastatic tumors (# organs) collected at autopsy	25 (5)	17 (5)	14 (4)	21 (5)	16 (4)

Note: All patients had extensive smoking history, metastatic disease at time of diagnosis, received standard of care platinum-doublet chemotherapy, radiation therapy, and had partial response except for one patient. All patients received more than one line of therapy, including experimental therapies on clinical trials as indicated in the footnote. Patients who received experimental therapies were non-responders.
[a]Prophylactic cranial irradiation
[b]Partial response
[c]Clinical trial NCT02674568: Study of Rovalpituzumab Tesirine (SC16LD6.5) for Third-line and Later Treatment of Subjects With Relapsed or Refractory Delta-Like Protein 3-Expressing Small Cell Lung Cancer (TRINITY)
[d]Clinical trial NCT02538666: An Investigational Immuno-therapy Study of Nivolumab, or Nivolumab in Combination with Ipilimumab, or Placebo in Patients with Extensive-Stage Disease Small Cell Lung Cancer (ED-SCLC) After Completion of Platinum-based Chemotherapy (CheckMate 451)

mutations per megabase of genome (Supplementary Data 2–6). The percentage of private somatic variants, or those present in only one tumor sample, in patients 1 to 5 ranged from 32% to 56%, suggesting high intertumoral heterogeneity (Supplementary Fig. 1A and B). We assessed the identities of SMGs using MuSiC,[27] finding *TP53* as the top SMG mutated in 100% of the tumor samples (Fig. 1A). Additional SMGs included *LRP1B*, *RYR2*, and *USH2A* (Fig. 1A and Supplementary Data 7). We sought to determine whether these genes may be preferentially mutated in SCLC relative to other cancer types by assessing their alteration frequency in The Cancer Genome Atlas PanCancer Atlas studies (>10,000 samples) and 210 predominantly primary SCLC samples[7–9,13] through cBioPortal for Cancer Genomics.[36,37] This analysis revealed a high-alteration frequency of these genes in SCLC but also in other cancer types with high TMB (Supplementary Fig. 2A and B).

We detected an *RB1* E204X nonsense mutation in a subset of tumor samples in patient 5 (Supplementary Data 6), and *PTEN* mutations in patients 1 and 3. In patient 1, *PTEN* C105F (a validated driver variant) was present in all metastatic tumor samples except for a residual primary right lung tumor and three brain metastases (Supplementary Data 2). In patient 3, *PTEN* Y46N was present in a single metastatic tumor sample (Supplementary Data 4).

CNVs in Relapsed SCLC

We identified a high frequency of CNVs using FALCON[24] in all SCLC tumor samples from the five autopsy patients (Fig. 1B, Supplementary Data 8). All patients had monoallelic loss, defined as allele copy less than 0.5, of chromosome 17p regions containing *TP53*. We also detected monoallelic loss of chromosome 13q regions containing *RB1* in patients 2, 3, and 5. Notably, tumor samples from all five patients had monoallelic deletions of a region on chromosome 5q containing *APC*. Consistent with previous studies,[8] we detected allele-specific gains, defined as allele copy greater than 2, of chromosome 3q regions containing *SOX2* in patients 1, 3, and 5; and 8q regions containing *MYC* in patients 1, 3, and 4.

Clonal Heterogeneity and Evolution in Relapsed SCLC

We used the tool CANOPY[25] to integrate single-nucleotide variant (SNVs), indels, and curated CNVs (Supplementary Fig. 2C) to infer clonal diversity and architecture in advanced SCLC.[18] Between 5 and 8 genetically distinct tumor cell clones were inferred to exist in each patient (Figs. 2A–D and 3A, Supplementary Data 9). *TP53* and *RB1* mutations were classified as truncal in all patients. Mutations in epigenetic modifiers such as *CREBBP* and *HDAC2* were also truncal, along

with *APC* (5q) deletion in a subset of patients. Subclonal alterations included *PTEN* deletion and mutations and *MYC* amplification. We used CHASM[28] to identify predicted driver mutations in Wnt pathway genes such as *XPO1* and *AXIN1* (Supplementary Data 10). We used Bradley-Terry models[18] to approximate the temporal occurrence of clonal and subclonal alterations and found that truncal alterations in *TP53*, *RB1*, *CREBBP*, and *HDAC2* occurred early, consistent with the critical role of these tumor suppressors in SCLC biology (Supplementary Data 11). Finally, we used deconstructSigs[26] to analyze mutational signatures and found truncal signature 4, which is associated with tobacco smoking.[38]

We next evaluated spatiotemporal clonal heterogeneity in advanced SCLC. In patient 1, we identified a tumor cell clone (clone 4) unique to brain metastases (T3–5) and the remnant primary tumor (*T1) (Fig. 2A). In patient 2, the biopsy and posttreatment samples had similar clonal compositions (Fig. 2B). In patient 3, clone 5 in the biopsy sample decreased substantially in all but three (T7–9) posttreatment tumors corresponding to the brain and upper lung (Fig. 2C). Conversely, clone 6 in the biopsy sample substantially increased in a subset of posttreatment tumors, particularly in the lymph node samples T10 to 12. In patient 4, clone 3 harboring a *BRCA2* G620E mutation decreased considerably in all posttreatment tumor samples (T1–12) (Fig. 2D), consistent with the well-characterized platinum-sensitizing effects of *BRCA* mutations. Furthermore, posttreatment tumors had increased proportions of clones 4 to 6 that contained predicted driver alterations by CHASM in the Wnt pathway (*AXIN1* mutation, *APC* deletion), which has been associated with chemoresistance.[14]

Finally, in patient 5, we identified a tumor cell clone (clone 5) present at increased proportions in all six liver metastases (T6–11; Fig. 3A). In addition, ctDNA was isolated from the plasma of this patient shortly before death and subjected to WES (Supplementary Data 12). We determined high concordance ($p < 10^{-5}$) between ubiquitous tumor variants and ctDNA variants, including SNVs (Fig. 3B, Supplementary Fig. 3A) and indels (Supplementary Fig. 3B and C). To infer the abundance of clones identified from autopsy in ctDNA, we used a maximum likelihood approach that revealed similar clonal composition between ctDNA (ctDNA, Fig. 3A) and liver metastases, thus suggesting this patient's hepatic tumor burden preferentially contributed to ctDNA.

RNA-Seq Reveals Decreased Antitumor Immunity in Advanced SCLC

To further characterize advanced SCLC, we performed transcriptome sequencing on a subset of tumor
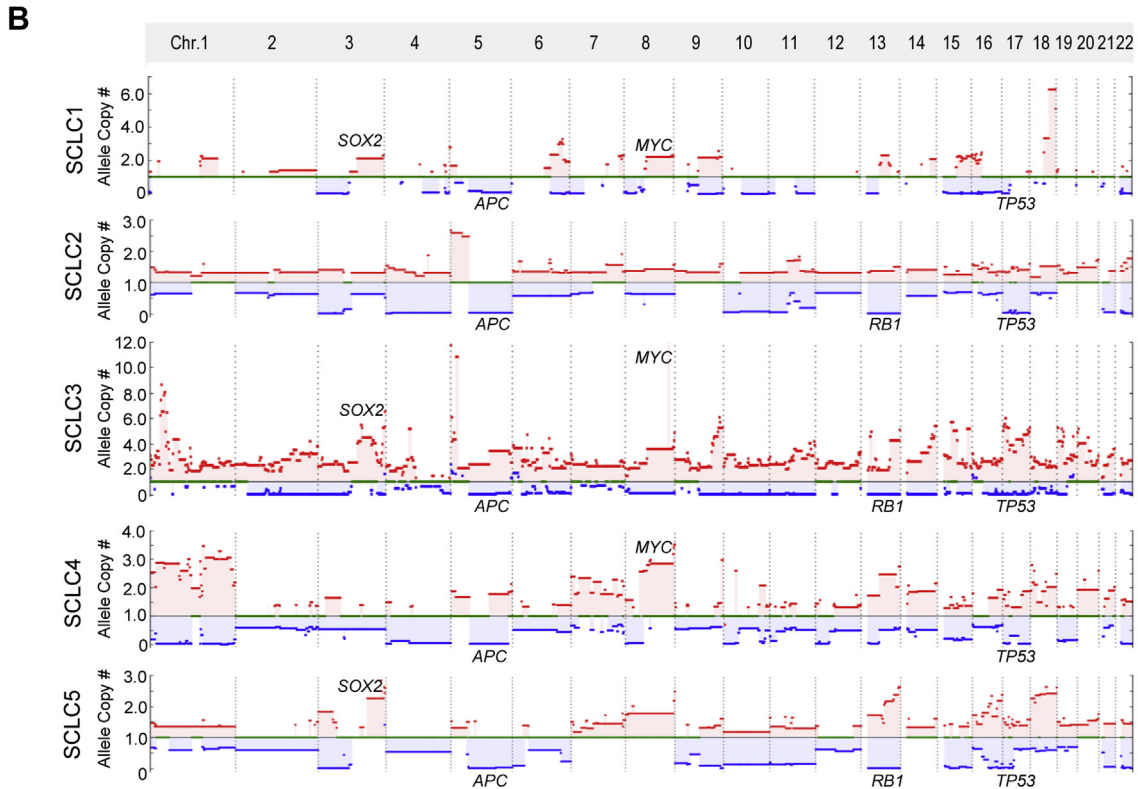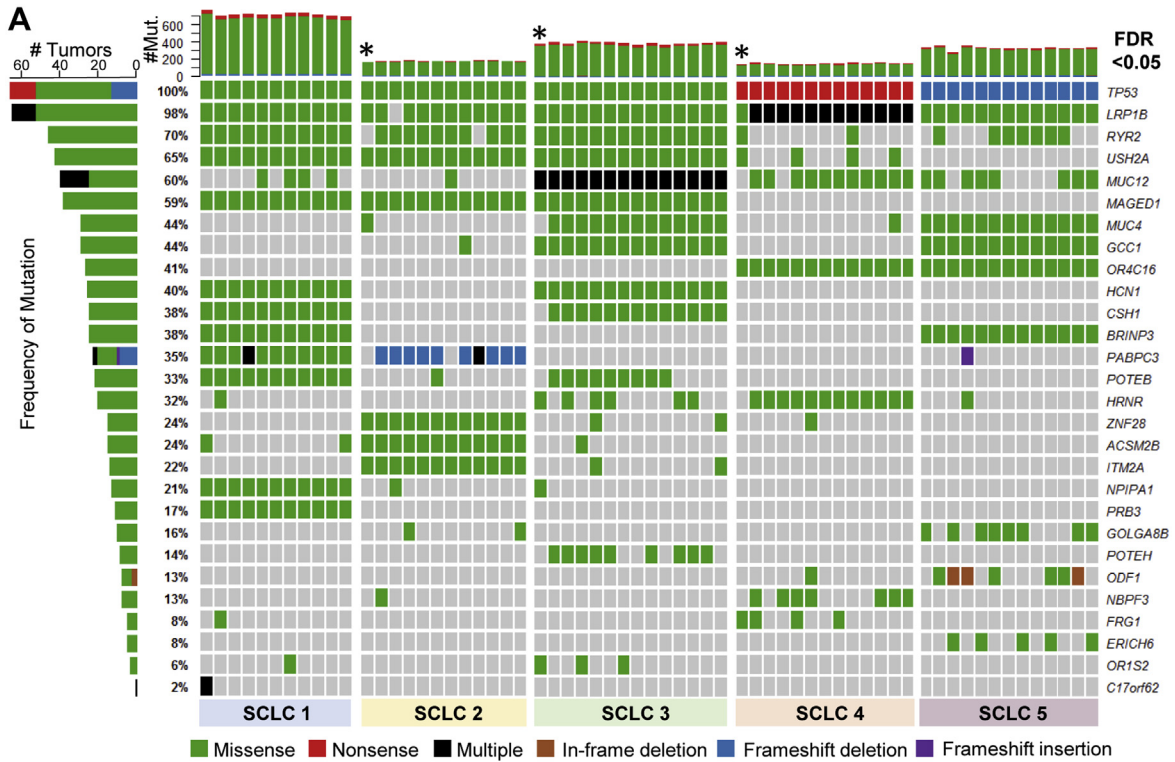
Figure 1. Identification of SMGs and CNVs in SCLC autopsy patients. (*A*) Oncoplot of SMGs identified in our SCLC cohort using MuSiC (FDR < 0.05). Multiple tumor samples per patient with SCLC were sequenced, resulting in exome data from 63 samples including three pretreatment biopsy samples (marked by *). Vertical bar graphs (top) reveal total number of Mut. per corresponding tumor sample below. Horizontal bar graphs and percentages (left) reveal mutational frequency of the corresponding gene (right). Type of somatic variant is defined by colored box key at the bottom, with black boxes indicating multiple variants detected in a specific gene in a given tumor sample. (*B*) Uncurated CNVs in SCLC autopsy patients detected by FALCON. Data from all tumor samples per patient were pooled into a composite CNV profile as illustrated for each patient. Gains were defined as allele number greater than 2.0 (e.g., *SOX2*) and loss less than 0.5 (e.g., *APC*). Red line, major allele. Blue line, minor allele. Green line, no change in one or both alleles. CNV, copy number variation; FDR, false discovery rate; Mut., mutation; SMG, significantly mutated gene. #, number.
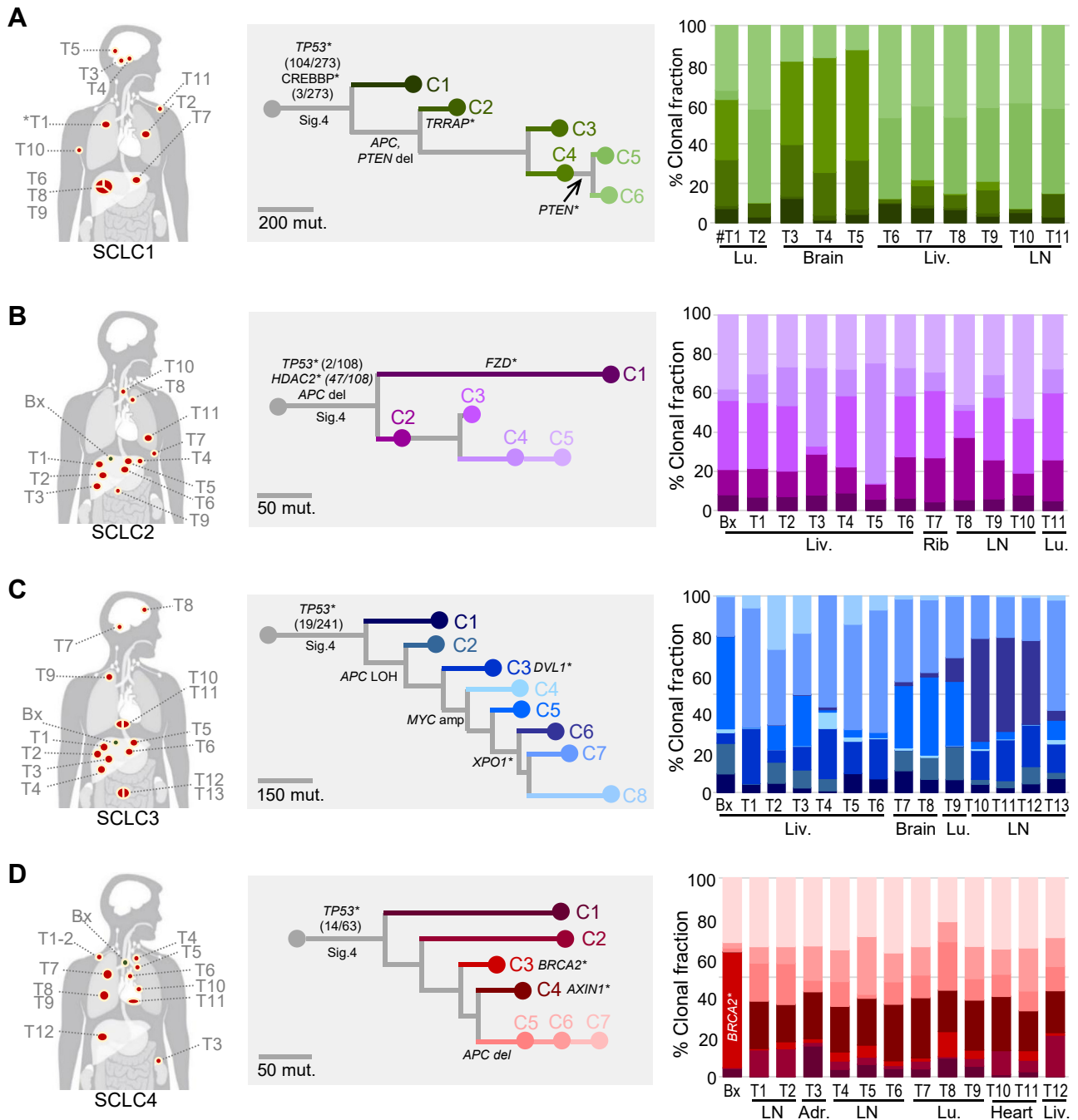
Figure 2. Inferred clonal phylogeny and heterogeneity in four SCLC autopsy patients. (*A-D*) (Left) Tumor samples procured from research autopsy as labeled on the human figure. Three large tumors from SCLC1 and SCLC3 were divided into multiple regions for sequencing. (*A-D*) (Middle) Phylogenetic trees depicting clonal evolution from a normal cell (gray solid circle) are as illustrated, with branch length corresponding to mutational burden. Numbers in parentheses after genes reveal predicted order of occurrence in a truncal branch (e.g., *A*, *CREBBP*, third mut. to occur of 273 truncal alterations). The COSMIC tobacco mut. Sig.4 was detected in the trunk of all five phylogenetic trees. Clonal and subclonal predicted driver mut., indicated by *, in Wnt signaling genes include *CREBBP* and *TRRAP* in (*A*) SCLC1, (*B*) *FZD* in SCLC2, *DVL1*, and (*C*) *XPO1* in SCLC3, and (*D*) *AXIN1* in SCLC4. (*A-D*) (Right) Percentage of different clones that compose each tumor sample are as revealed, demonstrating increased clonal heterogeneity. #T1, residual primary tumor in SCLC1; Adr., adrenal; Bx, pretreatment biopsy; del, deletion; Liv., liver; LN, lymph node; LOH, loss of heterozygosity; Lu, lung; mut., mutation; Sig., signature.

samples from each SCLC autopsy patient (Supplementary Data 1). Given the limited number of matched lung normal and pretreatment/primary SCLC tumors in our data set, we incorporated additional publicly available SCLC RNA-seq data sets[8,14,15,33] into all subsequent analyses. Two external SCLC data sets combined had 31
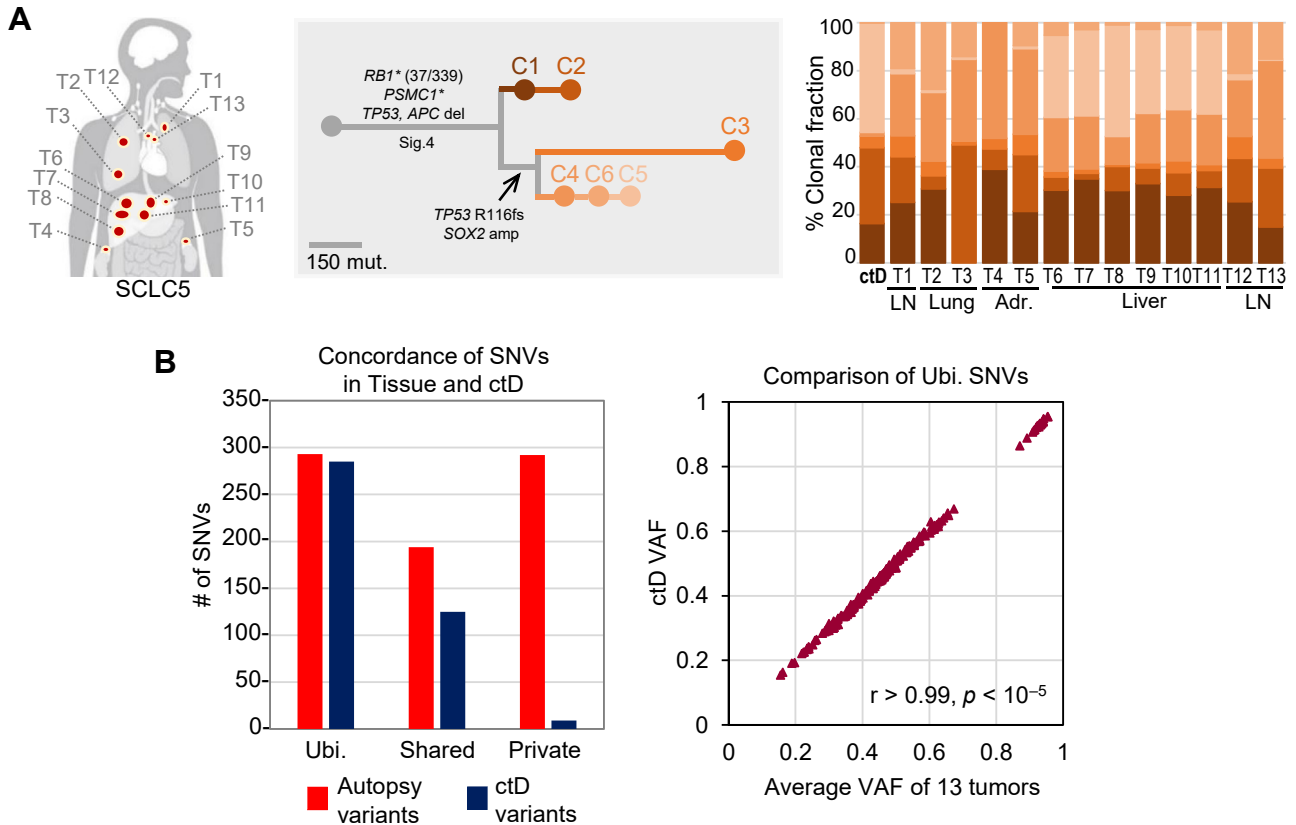
Figure 3. Concordance between ctD (ctDNA) and tumor profiling in a fifth SCLC autopsy patient. (*A*) Inferred clonal phylogeny and clonal composition of metastatic tumors from a fifth SCLC autopsy patient. Truncal predicted driver alterations include point mut. in *RB1* and Wnt pathway gene *PSMC1* and copy number losses of *TP53* and *APC*. Tumor clonal heterogeneity was recapitulated in a ctD sample collected shortly before death of this patient. The ctD sample revealed a high proportion of clone 5, which was detected in increased proportions only in liver metastases T6 to T11. (*B*) (Left) Bar graph reveals concordant numbers of SNVs between tumor and ctD. (Right) Average VAF of Ubi. SNVs was compared with VAF of ctD variants. amp, amplification; ctD, circulating tumor DNA; del, deletion; mut., mutation; Sig., signature; SNV, single-nucleotide variant; Ubi., ubiquitous; VAF, variant allele frequency. #: number.

relapsed and three pretreatment samples,[14,15] one data set contained 30 primary SCLC and 25 matched normal samples,[8] and one data set contained eight normal lung samples.[33] We first performed ssGSEA[31] using gene sets from the NanoString Tumor Signaling 360 panel (Supplementary Data 13). Intriguingly, most SCLC samples had decreased enrichment of pathways related to antitumor immune response: "avoiding immune destruction" and "tumor-promoting inflammation" compared with normal samples (Supplementary Fig. 4A).

To delineate how the immune tumor microenvironment (TME) may be altered in SCLC, we next performed ssGSEA using the NanoString PanCancer Immuno-Oncology 360 panel. This revealed decreased enrichment ($p < 0.001$) of processes annotated with adaptive antitumor immune function and immuno-metabolism in SCLC tumors relative to normal tissue (Fig. 4A, Supplementary Data 13). We also used ImSig[32] to

interrogate immune cell subsets in the SCLC TME, which revealed low gene expression signatures of T cells and innate immune cells in primary and relapsed SCLC tumors (Fig. 4B, Supplementary Data 13). Finally, we repeated ssGSEA and ImSig on our own research autopsy data set, in addition to the above-mentioned analyses of pooled data sets, and confirmed these results (Supplementary Fig. 4B and C).

T cells are key mediators of the adaptive antitumor immune response and targets of immune checkpoint inhibitors (ICIs). Given that ssGSEA and ImSig results indicated decreased T cell presence in the SCLC TME, we further interrogated expression of 18 genes in the analytically validated T cell-inflamed GEP, which was developed as a predictor of clinical benefit to ICI in multiple cancer types.[39] Responders to ICI were reported to have pretreatment baseline tumors with higher GEP scores (hot), whereas nonresponders had tumors with lower baseline GEP scores (cold).[35,39]
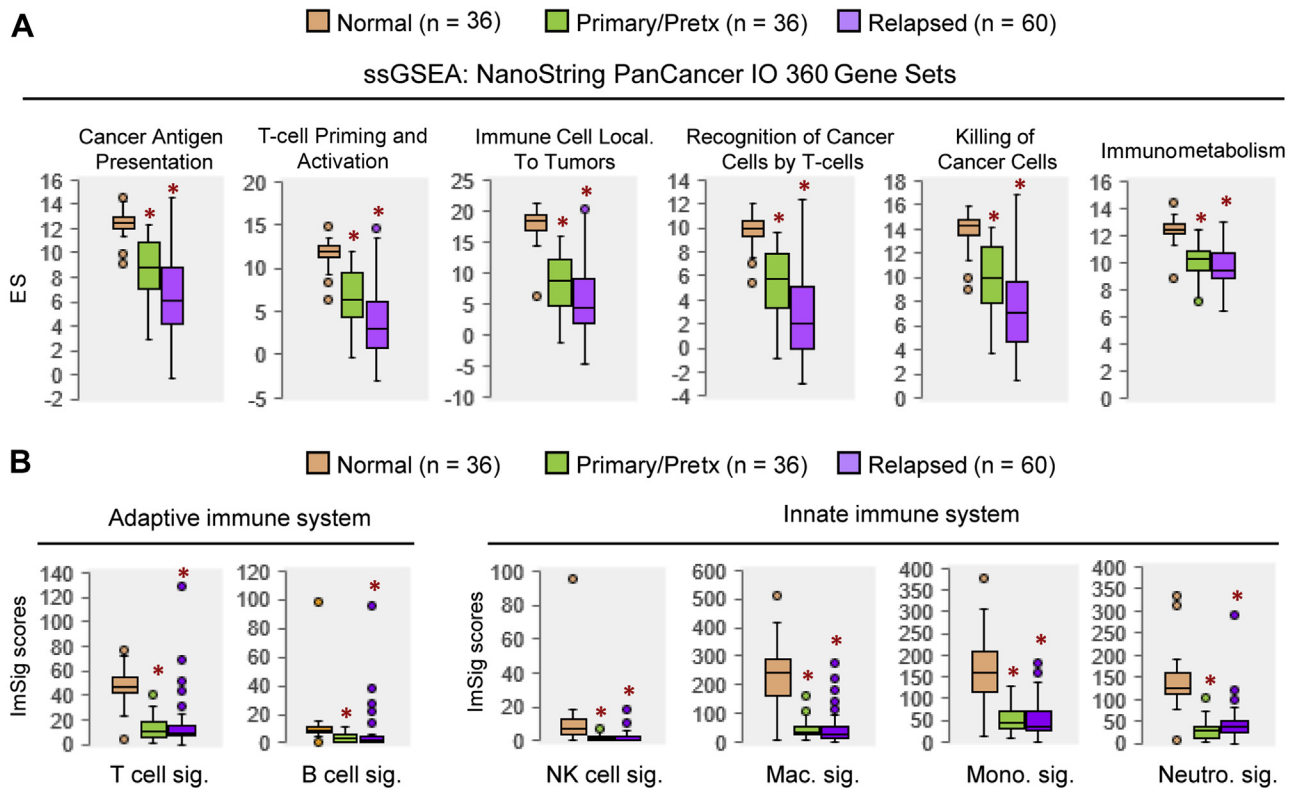
Figure 4. Transcriptome analyses reveal decreased expression of genes involved in antitumor immune responses in SCLC. (*A*) Box plots of ESs from ssGSEA analysis of gene sets derived from NanoString PanCancer IO 360 panel. Statistically significant differences in ES were detected in pairwise comparisons between normal-primary and normal-relapse. *, adjusted $p < 0.0001$. (*B*) Box plots of ImSig scores for different immune cell types in the adaptive and innate immune systems. Statistically significant differences in ES were detected in pairwise comparisons between normal-primary and normal-relapse. *, adjusted $p < 0.0001$. ES, enrichment score; ImSig, Immune signature; IO, Immune-Oncology; Mac., macrophage; Mono., monocyte; Neutro., neutrophil; NK, natural killer; Pretx, pretreatment; sig., signature; ssGSEA, single-sample gene set enrichment.

Hierarchical clustering (Fig. 5*A*, $p = 0.05$) and calculation of GEP scores in the pooled (Fig. 5*B*) and autopsy only (Supplementary Fig. 5*A*) data sets revealed that most primary and relapsed SCLC are cold relative to either matched tissue normal or non-SCLC subtypes of adenocarcinoma and squamous cell carcinoma (Supplementary Fig. 5*B*, Supplementary Data 14). Only five SCLC tumors were inflamed and had GEP scores higher than the median score of −0.09 in normal samples (Supplementary Data 15).

As atezolizumab and durvalumab are both programmed death-ligand 1 (PD-L1) monoclonal antibodies approved in combination with chemotherapy in advanced SCLC, we evaluated the expression of PD-L1 (*CD274*). *CD274* expression was low in most primary and relapsed SCLC samples (Fig. 5*C*, Supplementary Fig. 5*C*), consistent with previous analyses revealing that only a few patients (∼20%) with SCLC had tumors with PD-L1 protein expression greater than 1%.[40] In contrast to *CD274*, the expression of immune checkpoint inhibitory ligands *CD276* (*B7-H3*) and *CD200* was

increased in most SCLC tumor samples (Fig. 5*C*, Supplementary Fig. 5*C*). Consistent with ImSig revealing a lack of T cell signature in their TME, SCLC tumor samples had low expression levels of *CTLA4*, *TIGIT*, and other immune checkpoint molecules found on T cells (Fig. 5*C*, Supplementary Fig. 5*C*). Fially, interrogation of 50 SCLC cell lines from the Cancer Cell Line Encyclopedia recapitulated these gene expression patterns of *CD276*, *CD200*, and *CD274* (Supplementary Fig. 5*D*, Supplementary Data 14).

We further evaluated whether the four SCLC subtypes, as defined by the expression of *ASCL1*, *NEUROD1*, *YAP1*, and *POU2F3* using a previously described method[10] (Supplementary Fig. 6) and on the basis of highest gene expression evaluation (Supplementary Data 16), may have different immune phenotypes. As expected, most (n = 56 of 94) SCLC samples were *ASCL1*-high, whereas tumors with high expression of *ASCL1/-NEUROD1* (n = 11), *NEUROD1* (n = 13), *YAP1* (n = 6), and *POU2F3* (n = 8) were the minority. Hierarchical clustering revealed that the non-neuroendocrine SCLC
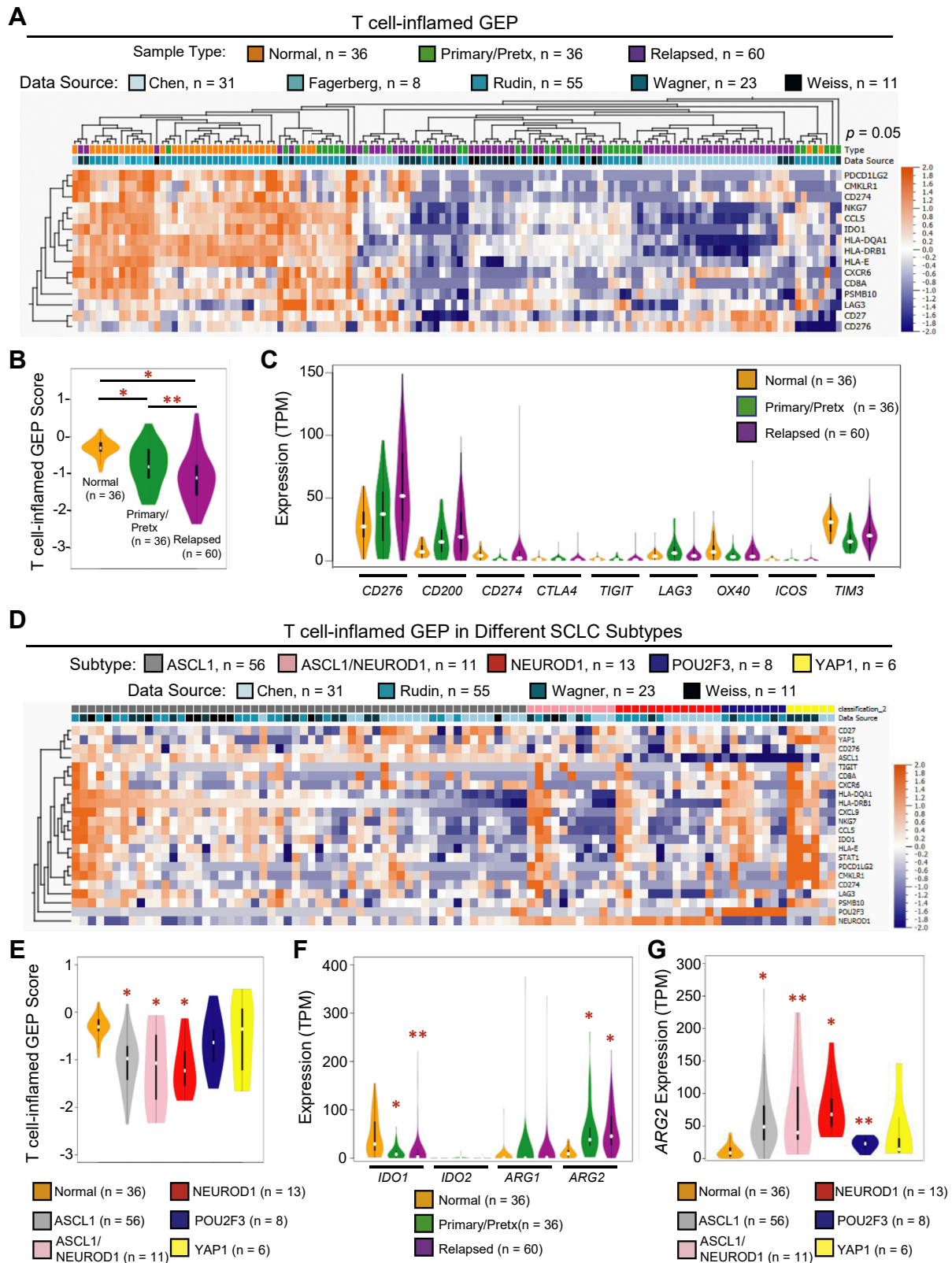
Figure 5. T cell-inflamed GEP evaluation reveals different immune phenotypes in neuroendocrine versus non-neuroendocrine SCLC. (*A*) Heatmap of log-transformed expression values (TPM) of genes representing the analytically validated T cell-inflamed GEP. Hierarchical clustering was performed using Qlucore Omics Explorer v3.6. Most primary and relapsed SCLC tumor samples revealed low GEP expression relative to normal lung tissue. Sample type and data source indicated as labeled. (*B*) Violin plot of GEP scores for normal, primary, and relapsed SCLC samples. Higher scores indicate "hot" tumors, whereas

subtypes, *YAP1* and *POU2F3*, had more tumors with elevated T cell-inflamed GEP whereas the classic and variant neuroendocrine subtypes were associated with predominantly low GEP (Fig. 5*D*). When GEP scores were calculated for each subtype,[35] *YAP1* and *POU2F3* tumors had GEP scores closer to that of normal lung tissue (Fig. 5*E*). *ImSig* analysis further revealed that *YAP1* tumors, although limited in sample size, are particularly associated with increased T cell and innate immune cell signatures (Supplementary Fig. 7).

Finally, to extend our analysis of suppressed immune function in SCLC, we interrogated expression of immunometabolism genes (Fig. 4*A*) encoding indoleamine 2,3-dioxygenase and arginase (ARG)1/2 enzymes (Fig. 5*F*), whose metabolic function have been reported to inhibit effector T cell and natural killer cell activity.[41–43] Of the four genes, only *ARG2* expression was significantly increased in primary and relapsed SCLC tumors (Fig. 5*F*) and cell lines (Supplementary Fig. 5*D*). We then evaluated *ARG2* expression on the basis of SCLC subtypes (Fig. 5*G*) and in NSCLC (Supplementary Fig. 8*A* and *B*). This analysis revealed high *ARG2* expression in the neuroendocrine SCLC subtypes (*ASCL1*, *ASCL1/NEUROD1*, and *NEUROD1*) and low *ARG2* expression in the non-neuroendocrine subtypes (*YAP1* and *POU2F3*) (Fig. 5*G*) and low *ARG2* expression in NSCLC (Supplementary Fig. 8*B*). Taken together, these results support the need to further investigate *ARG2* as a potential negative regulator of immune TME in the most common neuroendocrine SCLC subtypes.

Discussion

In this study, we leveraged rapid research autopsy to perform genomic and transcriptomic characterization of advanced SCLC. Our results revealed substantial clonal heterogeneity in relapsed SCLC, arising through branched evolution. We identified numerous subclonal alterations likely underlying treatment sensitivity, thus explaining the expansion or reduction of specific clones in tumors at different metastatic sites in each patient. Although limited in sample size, our results revealed that certain clones are enriched in metastatic sites such as the brain and liver, with the liver as the main ctDNA contributor in one patient. The ability to detect tissue-specific clones may have certain clinical use. For example, the central nervous system (CNS) is a frequent site of metastasis in patients with SCLC. The presence of brain-specific subclonal alterations in the ctDNA may help predict which patients are at highest risk for CNS disease and therefore be considered for prophylactic cranial irradiation or novel therapies to prevent CNS disease. Our study demonstrates the use of autopsy in studying subclone preference for specific metastatic niches, which will require additional autopsies of patients with SCLC and other solid tumors.

In addition to identifying *TP53* as the top SMG and inferring *TP53* mutations as truncal drivers in all autopsy patients, we also identified multiple mutations in *LRP1B*, which has putative tumor-suppressor functions.[44–46] These truncal alterations raise the possibility that *LRPB1*-mutant tumor cells may acquire an early fitness advantage over wild-type cells, which is further supported by an increased frequency of *LRP1B* mutations in primary SCLC tumor samples (Supplementary Fig. 1*A*). Thus, we propose that functional validation of variants in this gene and others (e.g., *RYR2*, *USH2A*) in appropriate model systems may begin to unravel their roles in the biology of SCLC and potentially other cancers.

Alterations in the Wnt signaling pathway have been linked to acquired chemoresistance in relapsed SCLC.[14] In a cohort of 30 relapsed SCLC samples, loss of heterozygosity of either *APC* or *CDH8* was detected in 23 of 30 samples, whereas mutations in either gene were detected in 10 of 30 samples. In our autopsy cohort, we identified copy number loss of *APC* as truncal or very early subclonal events in patients 1 to 3. We found truncal (*PSMC1*) and multiple subclonal (*TRRAP*, *FZD2*, and *XPO1*) predicted driver mutations in other Wnt signaling pathway genes. For instance, in patient 3, the autopsy tumor samples were enriched for clones C6 to C8 containing an *XPO1* mutation. In patient 4, mutation of another Wnt signaling gene, *AXIN1*, was assigned to a clone of tumor cells (C4) exclusively detected in post-treatment autopsy tumor samples. Therefore, our results are consistent with and support the established association between Wnt pathway and early chemoresistance in advanced SCLC.

Analysis of ctDNA in patients with advanced SCLC represents a valuable approach to tracking tissue-specific clones or emergence of resistant clones.[47]

---

lower scores indicate "cold" tumors. Two-tailed unpaired *t* test **p* < 0.001; ***p* < 0.01. (*C*) Violin plot of TPM values of selected T cell-inflamed GEP and checkpoint genes in normal and SCLC tumor samples. (*D*) Heatmap of log-transformed expression values (TPM) of T cell-inflamed GEP genes in SCLC tumor samples annotated by subtype and data source as indicated. (*E*) Violin plot of GEP scores in different subtypes of SCLC and normal lung. Each subtype was compared against normal using two-tailed unpaired *t* test *, *p* < 0.01. (*F*) Violin plot of *IDO1/2* and *ARG1/2* expression in normal, primary, and relapsed SCLC. Primary/pretx or relapsed samples were compared against normal using two-tailed unpaired *t* test **p* < 0.001; ***p* < 0.005. (*G*) Violin plot of *ARG2* expression in SCLC tumor samples annotated by subtype. Each subtype was compared against normal using two-tailed unpaired *t* test. **p* < 0.001; ***p* < 0.005. ARG, arginase; GEP, gene expression profile; IDO, indoleamine 2,3-dioxygenase; Pretx, pretreatment; TPM, transcript reads per million.

Although most studies have compared ctDNA with either a single primary or metastatic tumor biopsy, rapid autopsy enables the comparison of variants detected in ctDNA against variants in multiple metastatic tumors. In our study, we performed WES of ctDNA from patient 5 and detected nearly all ubiquitous tumor variants from autopsy that likely represented most of this patient's truncal variants (concordance 97%–100% for SNVs and indels). Not surprisingly, for variants that were classified as shared or private at autopsy (e.g., subclonal variants), the metastatic tumor-ctDNA concordance rates were much lower. Therefore, our results reveal effective detection of truncal variants in ctDNA, but considerable limitations for detecting subclonal variants. These data and future autopsy studies will provide important contributions toward refining the limits of ctDNA detection for clinical applications, including the evaluation of minimal residual disease and cancer recurrence.

Within our autopsy SCLC cohort, we performed transcriptome sequencing to evaluate whether mutations in SMGs may correlate with altered expression, thereby representing potential driver genes. However, this initial analysis did not reveal a significant correlation. In addition, consistent with previous studies revealing a paucity of gene fusions as drivers in SCLC,[48] we did not detect any putative fusions that were recurrent in more than one tumor sample within our cohort. Recognizing that these results may be attributed to our limited cohort size, we incorporated external primary and relapsed SCLC RNA-seq data sets in subsequent analyses, which ultimately revealed suppressed immune TME in the neuroendocrine SCLC subtypes (*ASCL1*, *NEUROD1*, and *ASCL1/NEUROD1*).

Given that only approximately 20% of patients with SCLC have tumors expressing PD-L1 (>1% by immunohistochemistry),[40] improved characterization of the SCLC immune TME remains an unmet need, particularly given recent regulatory approvals of frontline PD-L1 blockade therapy. Our results confirmed low *CD274* (PD-L1) expression in most SCLC tumors and cell lines, supporting the above-mentioned clinical observations. Additional ssGSEA and ImSig analyses corroborated decreased adaptive antitumor immune function in primary and relapsed SCLC. Although we lacked outcomes data to correlate with T cell-inflamed GEP scores, which predicts clinical benefit to programmed cell death protein 1/PD-L1 blockade,[39] hierarchical clustering revealed a noninflamed phenotype in most primary and advanced SCLC. Interestingly, T cell-inflamed GEP expression was high, or close to that of normal lung samples, in non-neuroendocrine SCLC subtypes (*YAP1* and *POU2F3*) (Fig. 5D), which had low *ARG2* expression (Fig. 5E). In contrast, GEP expression was low in the neuroendocrine SCLC subtypes (*ASCL1, ASCL1/*

NEUROD1, and *NEUROD1*), which had high *ARG2* expression. Given these observations, we hypothesize that increased ARG2 expression and function may represent a cell-autonomous oncogenic metabolic adaptation enabling suppression of adaptive antitumor immunity in the SCLC TME independent of PD-L1 expression. These results will need to be validated in larger, independent data sets but suggest that subtyping patients with SCLC before systemic treatment should aid in the identification of patients most likely to benefit from chemo-ICI. Finally, it was recently reported that the non-neuroendocrine SCLC subtypes were more likely to be admixed SCLC and NSCLC,[11] which in addition to low *ARG2* expression may further explain the higher GEP scores and inflamed phenotype in these tumors given the responsiveness of NSCLC to ICI.

Continuing the analysis of immune TME, in addition to decreased *CD274* expression, we reported decreased expression of *CTLA4*, *LAG3*, *TIM3*, and other well-characterized immune checkpoint proteins in advanced SCLC. Conversely, we detected increased expression of alternate checkpoint molecules, *CD276* (*B7-H3*) and *CD200*. CD276 is a member of the B7 family, which also includes PD-L1 (B7-H1). Consistent with our finding of increased gene expression, CD276 protein expression was recently detected in 64.9% of a SCLC cohort with 90 patients.[49] The same study reported PD-L1 expression at a much lower rate of 7.3%.[49] CD276 is expressed at low levels in normal tissues but when aberrantly expressed on various tumor cell types contributes to T cell inhibition, tumor cell immune evasion, and is associated with poor prognosis.[50] Therefore, targeting CD276 is being explored as an immune-stimulatory strategy in cancer.[51] CD200 is a checkpoint molecule that leads to suppression of secretion of proinflammatory cytokines, including interleukin-2 and I interferon-γ.[52] Consistent with increased *CD200* expression in the SCLC samples we analyzed, CD200 protein was expressed in two other SCLC cohorts.[53,54] Furthermore, inhibiting the CD200 signaling axis has been reported to stimulate antigen-specific immune response against glioblastoma multiforme.[52] Therefore, these results support further exploration of targeting CD276 or CD200 in preclinical SCLC models to determine whether inhibiting these checkpoint pathways may yield viable therapeutic strategies for advanced SCLC.

As drug development efforts focus on programmed cell death protein 1/PD-L1 and other immune regulatory checkpoints, characterization of both the immune microenvironment and tumor heterogeneity will be critical to differentiate responders from nonresponders. It will also be important to define the relationship between tumor heterogeneity and neoantigen formation. For example, in NSCLC, cytotoxic tumor-infiltrating T

cells preferentially develop against clonal neoantigens (derived from clonal or truncal mutations) in patients with durable clinical benefit to ICI.[55] The high smoking-associated TMB of SCLC suggests that there may be a high number of clonal neoantigens serving as therapeutic targets. Therefore, a combination of autopsy and ctDNA samples will be critical resources to help characterize the prevalence of clonal neoantigens and optimize their detection from liquid biopsy. This will enable the development of vaccine or T cell-based therapeutic strategies in SCLC and other solid cancers.

In summary, we have partnered with patients for rapid research autopsy to study relapsed SCLC and performed extensive analyses of clonal heterogeneity, subclonal architecture, and the immune microenvironment. Our results suggest a potential explanation for why SCLC, a cancer with high TMB and thus potential tumor neoantigens, exhibits lower than expected response rates to ICI compared with other solid tumors with similar median TMB. Future studies using single-cell sequencing strategies will shed light on unanswered questions, including which cell types are the source of *ARG2* expression and whether CD200/CD276 are coexpressed. Metabolome profiling could identify additional metabolic vulnerabilities in SCLC that may be cotargeted to enhance ICI response. Innovative immunotherapeutic approaches targeting alternate checkpoints, potentially combined with isoform-specific ARG inhibition, may ultimately result in more robust clinical activity against advanced SCLC.

Acknowledgments

Supplementary Data

To access the supplementary material accompanying this article, visit the online version of the *JTO Clinical and Research Reports* at www.jtocrr.org and at https://doi.org/10.1016/j.jtocrr.2021.100164

References

1. Sabari JK, Lok BH, Laird JH, Poirier JT, Rudin CM. Unravelling the biology of SCLC: implications for therapy. *Nat Rev Clin Oncol*. 2017;14:549-561.
2. Siegel RL, Miller KD, Jemal A. Cancer statistics, 2019. *CA Cancer J Clin*. 2019;69:7-34.
3. Horn L, Mansfield AS, Szczęsna A, et al. First-line atezolizumab plus chemotherapy in extensive-stage small-cell lung cancer. *N Engl J Med*. 2018;379:2220-2229.
4. Paz-Ares L, Dvorkin M, Chen Y, et al. Durvalumab plus platinum-etoposide versus platinum-etoposide in first-line treatment of extensive-stage small-cell lung cancer (Caspian): a randomised, controlled, open-label, phase 3 trial. *Lancet*. 2019;394:1929-1939.
5. von Pawel J, Schiller JH, Shepherd FA, et al. Topotecan versus cyclophosphamide, doxorubicin, and vincristine for the treatment of recurrent small-cell lung cancer. *J Clin Oncol*. 1999;17:658-658.
6. Trigo J, Subbiah V, Besse B, et al. Lurbinectedin as second-line treatment for patients with small-cell lung cancer: a single-arm, open-label, phase 2 basket trial. *Lancet Oncol*. 2020;21:645-654.
7. George J, Lim JS, Jang SJ, et al. Comprehensive genomic profiles of small cell lung cancer. *Nature*. 2015;524:47-53.
8. Rudin CM, Durinck S, Stawiski EW, et al. Comprehensive genomic analysis identifies SOX2 as a frequently amplified gene in small-cell lung cancer. *Nat Genet*. 2012;44:1111-1116.
9. Peifer M, Fernández-Cuesta L, Sos ML, et al. Integrative genome analyses identify key somatic driver mutations of small-cell lung cancer. *Nat Genet*. 2012;44:1104-1110.
10. Rudin CM, Poirier JT, Byers LA, et al. Molecular subtypes of small cell lung cancer: a synthesis of human and mouse model data. *Nat Rev Cancer*. 2019;19:289-297.
11. Baine MK, Hsieh MS, Lai WV, et al. SCLC subtypes defined by ASCL1, NEUROD1, POU2F3 and YAP1: a comprehensive immunohistochemical and histopathologic characterization. *J Thorac Oncol*. 2020;15:1823-1835.
12. Gay CM, Stewart CA, Park EM, et al. Patterns of transcription factor programs and immune pathway activation define four major subtypes of SCLC with distinct therapeutic vulnerabilities. *Cancer Cell*. 2021;39:346-360.e7.

13. Gardner EE, Lok BH, Schneeberger VE, et al. Chemo-sensitive relapse in small cell lung cancer proceeds through an EZH2-SLFN11 axis. *Cancer Cell*. 2017;31:286-299.

14. Wagner AH, Devarakonda S, Skidmore ZL, et al. Recurrent WNT pathway alterations are frequent in relapsed small cell lung cancer. *Nat Commun*. 2018;9:3787.

15. Weiss GJ, Byron SA, Aldrich J, et al. A prospective pilot study of genome-wide exome and transcriptome profiling in patients with small cell lung cancer progressing after first-line therapy. *PLoS One*. 2017;12:e0179170.

16. Stewart CA, Gay CM, Xi Y, et al. Single-cell analyses reveal increased intratumoral heterogeneity after the onset of therapy resistance in small-cell lung cancer. *Nat Cancer*. 2020;1:423-436.

17. Krook MA, Chen HZ, Bonneville R, Allenby P, Roychowdhury S. Rapid research autopsy: piecing the puzzle of tumor heterogeneity. *Trends Cancer*. 2019;5:1-5.

18. Krook MA, Bonneville R, Chen HZ, et al. Tumor heterogeneity and acquired drug resistance in FGFR2-fusion-positive cholangiocarcinoma through rapid research autopsy. *Cold Spring Harb Mol Case Stud*. 2019;5:1-5.

19. Reeser JW, Martin D, Miya J, et al. Validation of a targeted RNA sequencing assay for kinase fusion detection in solid tumors. *J Mol Diagn*. 2017;19:682-696.

20. Griffith M, Miller CA, Griffith OL, et al. Optimizing cancer genome sequencing and analysis. *Cell Syst*. 2015;1:210-223.

21. Li H, Durbin R. Fast and accurate short read alignment with Burrows-Wheeler transform. *Bioinformatics*. 2009;25:1754-1760.

22. McKenna A, Hanna M, Banks E, et al. The Genome Analysis Toolkit: a MapReduce framework for analyzing next-generation DNA sequencing data. *Genome Res*. 2010;20:1297-1303.

23. Koboldt DC, Zhang Q, Larson DE, et al. VarScan 2: somatic mutation and copy number alteration discovery in cancer by exome sequencing. *Genome Res*. 2012;22:568-576.

24. Chen H, Bell JM, Zavala NA, Ji HP, Zhang NR. Allele-specific copy number profiling by next-generation DNA sequencing. *Nucleic Acids Res*. 2015;43:e23.

25. Jiang Y, Qiu Y, Minn AJ, Zhang NR. Assessing intratumor heterogeneity and tracking longitudinal and spatial clonal evolutionary history by next-generation sequencing. *Proc Natl Acad Sci U S A*. 2016;113:E5528-E5537.

26. Rosenthal R, McGranahan N, Herrero J, Taylor BS, Swanton C. DeconstructSigs: delineating mutational processes in single tumors distinguishes DNA repair deficiencies and patterns of carcinoma evolution. *Genome Biol*. 2016;17:31.

27. Dees ND, Zhang Q, Kandoth C, et al. MuSiC: identifying mutational significance in cancer genomes. *Genome Res*. 2012;22:1589-1598.

28. Carter H, Chen S, Isik L, et al. Cancer-specific high-throughput annotation of somatic mutations: computational prediction of driver missense mutations. *Cancer Res*. 2009;69:6660-6667.

29. Kim D, Paggi JM, Park C, Bennett C, Salzberg SL. Graph-based genome alignment and genotyping with HISAT2 and HISAT-genotype. *Nat Biotechnol*. 2019;37:907-915.

30. Kovaka S, Zimin AV, Pertea GM, Razaghi R, Salzberg SL, Pertea M. Transcriptome assembly from long-read RNA-seq alignments with StringTie2. *Genome Biol*. 2019;20:278.

31. Barbie DA, Tamayo P, Boehm JS, et al. Systematic RNA interference reveals that oncogenic KRAS-driven cancers require TBK1. *Nature*. 2009;462:108-112.

32. Nirmal AJ, Regan T, Shih BB, Hume DA, Sims AH, Freeman TC. Immune cell gene signatures for profiling the microenvironment of solid tumors. *Cancer Immunol Res*. 2018;6:1388-1400.

33. Fagerberg L, Hallström BM, Oksvold P, et al. Analysis of the human tissue-specific expression by genome-wide integration of transcriptomics and antibody-based proteomics. *Mol Cell Proteomics*. 2014;13:397-406.

34. Best SA, Hess JB, Souza-Fonseca-Guimaraes F, et al. Harnessing natural killer immunity in metastatic SCLC. *J Thorac Oncol*. 2020;15:1507-1521.

35. Cristescu R, Mogg R, Ayers M, et al. Pan-tumor genomic biomarkers for PD-1 checkpoint blockade–based immunotherapy. *Science*. 2018;362:eaar3593.

36. Cerami E, Gao J, Dogrusoz U, et al. The cBio cancer genomics portal: an open platform for exploring multi-dimensional cancer genomics data. *Cancer Discov*. 2012;2:401-404.

37. Gao J, Aksoy BA, Dogrusoz U, et al. Integrative analysis of complex cancer genomics and clinical profiles using the cBioPortal. *Sci Signal*. 2013;6:pl1.

38. Forbes SA, Beare D, Boutselakis H, et al. COSMIC: somatic cancer genetics at high-resolution. *Nucleic Acids Res*. 2016;45:D777-D783.

39. Ayers M, Lunceford J, Nebozhyn M, et al. IFN-γ-related mRNA profile predicts clinical response to PD-1 blockade. *J Clin Invest*. 2017;127:2930-2940.

40. Iams WT, Porter J, Horn L. Immunotherapeutic approaches for small-cell lung cancer. *Nat Rev Clin Oncol*. 2020;17:300-312.

41. O'Sullivan D, Sanin DE, Pearce EJ, Pearce EL. Metabolic interventions in the immune response to cancer. *Nat Rev Immunol*. 2019;19:324-335.

42. Wang D, Saga Y, Mizukami H, et al. Indoleamine-2,3-dioxygenase, an immunosuppressive enzyme that inhibits natural killer cell function, as a useful target for ovarian cancer therapy. *Int J Oncol*. 2012;40:929-934.

43. Grzywa TM, Sosnowska A, Matryba P, et al. Myeloid cell-derived arginase in cancer immune response. *Front Immunol*. 2020;11:938.

44. Beer AG, Zenzmaier C, Schreinlechner M, et al. Expression of a recombinant full-length LRP1B receptor in human non-small cell lung cancer cells confirms the postulated growth-suppressing function of this large LDL receptor family member. *Oncotarget*. 2016;7:68721-68733.

45. Prazeres H, Torres J, Rodrigues F, et al. Chromosomal, epigenetic and microRNA-mediated inactivation of LRP1B, a modulator of the extracellular environment of thyroid cancer cells. *Oncogene*. 2017;36:146.

46. Wang Z, Sun P, Gao C, et al. Down-regulation of LRP1B in colon cancer promoted the growth and migration of cancer cells. *Exp Cell Res*. 2017;357:1-8.

47. Nong J, Gong Y, Guan Y, et al. Circulating tumor DNA analysis depicts subclonal architecture and genomic evolution of small cell lung cancer. *Nat Commun*. 2018;9:3114.

48. Iwakawa R, Takenaka M, Kohno T, et al. Genome-wide identification of genes with amplification and/or fusion in small cell lung cancer. *Genes Chromosomes Cancer*. 2013;52:802-816.

49. Carvajal-Hausdorf D, Altan M, Velcheti V, et al. Expression and clinical significance of PD-L1, B7-H3, B7-H4 and TILs in human small cell lung Cancer (SCLC). *J Immunother Cancer*. 2019;7:65.

50. Dong P, Xiong Y, Yue J, Hanley SJB, Watari H. B7H3 as a promoter of metastasis and promising therapeutic target. *Front Oncol*. 2018;8:264.

51. Picarda E, Ohaegbulam KC, Zang X. Molecular pathways: targeting B7-H3 (CD276) for human cancer immunotherapy. *Clin Cancer Res Off J Am Assoc Cancer Res*. 2016;22:3425-3431.

52. Xiong Z, Ampudia Mesias E, Pluhar GE, et al. CD200 checkpoint reversal: a novel approach to immunotherapy. *Clin Cancer Res*. 2020;26:232-241.

53. Bohling SD, Davis E, Thompson K, Kussick SJ, Love J. Flow cytometric analysis of CD200 expression by pulmonary small cell carcinoma. *Cytometry B Clin Cytom*. 2016;90:493-498.

54. Love JE, Thompson K, Kilgore MR, et al. CD200 expression in neuroendocrine neoplasms. *Am J Clin Pathol*. 2017;148:236-242.

55. McGranahan N, Furness AJ, Rosenthal R, et al. Clonal neoantigens elicit T cell immunoreactivity and sensitivity to immune checkpoint blockade. *Science*. 2016;351:1463-1469.